Computational Model of a Respiratory Network

David B. Ramsay[1] and Jeffrey C. Smith[2]

[1]Biomedical Engineering Summer Internship Program, National Institute of Biomedical Imaging and Bioengineering, National Institutes of Health

[2]Cellular and Systems Neurobiology Section, Laboratory of Neural Control, National Institute of Neurological Disorders and Stroke, National Institutes of Health

Introduction

Respiratory activity in mammals is controlled by a group of rhythmically firing neuronal populations. The primary components of this system are located in the ventrolateral medulla, allowing detailed experimental analysis of relevant neurons using medullary slice preparations from neonatal and juvenile rodents. These data indicate that three specialized cell populations form the basic framework for respiratory pattern formation. The neuronal kernel responsible for rhythm generation has been identified in the pre-Botzinger complex (pre-BotC), connected by premotoneurons (preMNs) to the motoneurons (MNs) in the motor nucleus. PreMNs are functionally responsible for pattern formation and signal transmission, while MNs amplify the transmitted signal for motor output.

Relevant single-compartment computational models based on this research have been published, describing both pre-BotC neurons and motoneurons. In this paper, we will present a computational model that incorporates existing experimental data with previous single-compartment models in order to effectively model the network as a whole.

The three cell populations we have modeled form the foundation of respiratory pattern generation, however represent only a small piece of the entire ponto-medullary system. The three core populations are embedded in a large network which provides complex input to the fundamental neuronal groups. In addition, inhibitory and excitatory cell populations interact dynamically to produce variations in the integrated nerve outputs. While this model includes all cell populations involved in hypoglossal nerve output, phrenic and central vagus nerve activity also results from interaction of this core network with other excitatory and inhibitory neuron kernels.

Methods and Materials

All models were created using the Berkeley Madonna Dynamic Systems software package, available at http://www.berkeleymadonna.com/. Trails were run on an Apple PowerPC G5 running Mac OS X, version 10.4.11. Error tolerances for every simulation were $\leq 10^{-6}$.

Developing the Cell Models

All of the single cell models were developed using the Hogkin-Huxley single-compartment formalism. Each cell's dynamics were completely defined by an autonomous set of differential equations. The primary relation for each cell was derived from Kirchhoff's current law:

$$C\,(\mathrm{d}V/\mathrm{d}t) = -I_{\text{tot-}}$$

where C is the cell capacitance (pF), V is the membrane potential (mV), t is time (ms), and I is the total current through the membrane (pA). The composite currents in each cell vary based on cell specialization, and will be discussed in more detail below.

PRE-BOTC CELL:

The pre-BotC cells were based on the Model 1 formulation put forth in Butera, et al. (1999). This model includes an experimentally verified slow persistent Sodium (I_{NaP}) current into the cell, which is counteracted by a K^+ dominated leak current. The ratio of these two currents dictates the activity of the isolated cell, forcing it into one of three regimes: silent, bursting, or tonically spiking (see figure below).

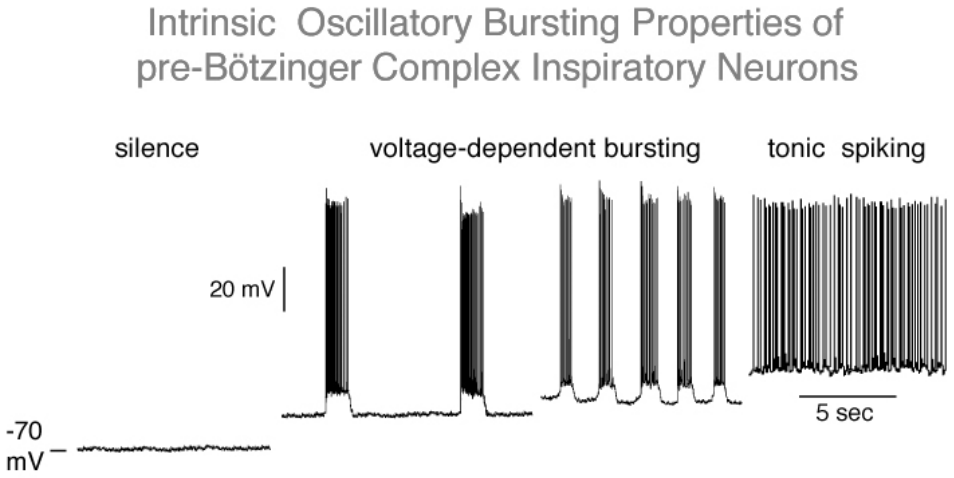

This characteristic of the pre-BotC cells is the source of the well documented spontaneous rhythmic activity in the respiratory network. The Model 1 formulation also has a fast sodium current (I_{Na}) and a delayed-rectifier Potassium current ($I\text{-}_K$). Each of these currents is governed by a reduced voltage-dependent formula of the form:

$$I = gx(V - E_{\text{reversal}})$$

where g is conductance (nS), x is a gating variable used to modulate the conductance, and E is the reversal potential for the ionic current (mV). The conductance value, measured experimentally, represents channel density. The x term takes several forms, from a simple voltage-dependent sigmoid, to several voltage-dependent variables interacting. The voltage gating characteristics for each ion are based

on experimental data. Taken together, these equations recreate pre-BotC cell behavior accurately. See Butera, et al. for more information about specific values, gating equations, or experimental justification of the model.

PRE-MN and MN CELLS:

Recent evidence has suggested that preMNs and MNs have similar biophysical and electrophysiological properties. While MNs are much larger cells, current densities and other volume-dependent properties between the two are equal. The action potential waveform and the underlying currents that govern its propagation are thus proportional to the size of the cell, which manifests itself in the single compartment model as cell capacitance.

The basis for both the preMNs and the MNs in this model was put forth in Purvis and Butera (2005). This single compartment model includes the persistent sodium current, the potassium dominated leak current, and the fast sodium and delayed-rectifier potassium currents. In addition, this single compartment model incorporates high- and low-voltage activated calcium currents (I_P, I_N and I_T), a voltage- and a calcium-dependent potassium current ($I\text{-}_A$ and $I\text{-}_{SK}$), and a hyperpolarization activated cationic current ($I_{H\text{-}\text{-}}$). Each of these currents has been documented experimentally, and are based on data taken from neonatal rat hypoglossal MNs. Though they have a persistent sodium current, they do not fire intrinsically because of a relatively higher balancing leak current. Thus, in order to test this model, applied current was required to stimulate the neuron into a spiking regime. This type of testing has verified that the model both responds accurately to changes in applied current (both through its adaptation and its steady-state firing frequency), and recreates the proper complex action potential waveform. This waveform, shown below, has characteristic fast afterhyperpolarization (fAHP), afterdepolarization (ADP), and medium-duration afterhyperpolarizatioin (mAHP) behavior.

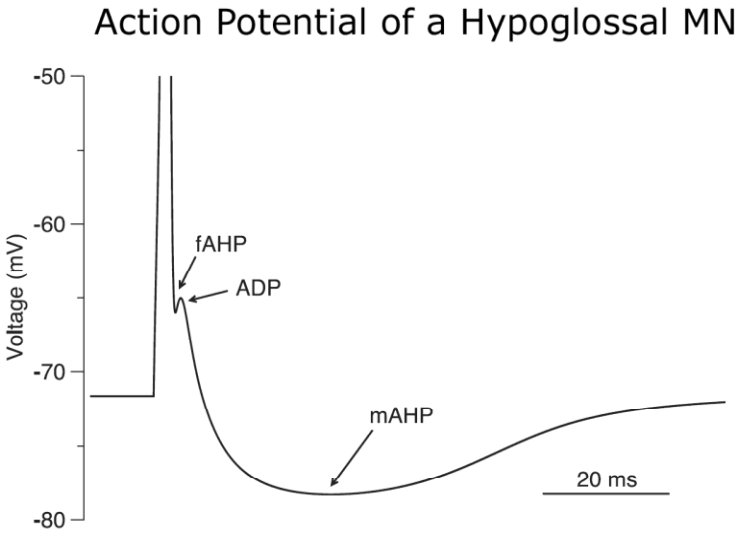

In order to preserve the properties of the original model, preMNs and MNs were created by scaling the ionic conductance coefficients of each new cell by the ratio of its capacitance to the capacitance of the existing model. Capacitances of 32.1 and 63.4 pF were used for the preMN and MN, respectively, as measured in Koizumi, et al. (2008). This technique preserved the relevant spike shape and current dynamics, while scaling the absolute properties of the cell to match the data.

RAPHE CELL:

The driving input to the three fundamental cell groups falls into two main divisions: a slow serotonergic input generated from the medullary raphe nucleus, and a faster glutamatergic tonic input extending from the pons. Studies of the raphe input have shown that these cells fire between 1 and 2 Hz, and have a unique spike shape (see figure below).

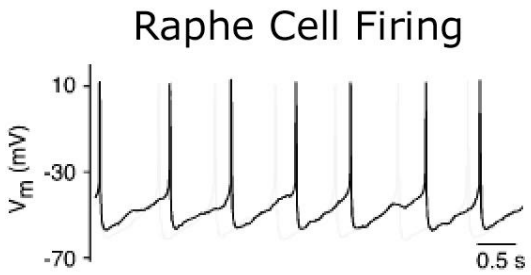

Development of these cells started with the fundamental currents responsible for generating an action potential— a fast sodium current and a delayed-rectifier Potassium current. A tonic drive (I_{tonic}) was then added, counterbalanced by a leak current (I_{leak}), which drove the cell into a spiking regime. Once the cell was spiking, modulation of g_{leak} was used to control the firing frequency, until it was in the expected range. In order to more accurately reflect the action potential shape and other experimental data, the additional currents found in the preMNs and MNs were added to this basic cell. Little specific data about ion currents exist for these cells, so conductance coefficients for each of the additional currents were varied until a reasonable spike shape was attained. A whole cell capacitance of 32.1 pF was used because Raphe neurons and preMNs are similarly sized.

OTHER TONIC INPUT:

Synaptic drive of the respiratory network is known to come from several other places besides the medullary raphe nucleus. Regions in the pons involved in respiration include the Kolliker-Fuse nucleus and the parabrachial complex dorsolaterally, as well as several ventrolateral areas. The medullary retrotrapezoid nucleus also provides respiratory drive, though no specific information on any of these areas exists. In order to properly include their effect, a new current was introduced to every cell (I_{tonic}), with a reversal potential of 0 mV (the potential of the presumed synaptic currents involved, non-*N*-methyl-D-aspartate EAA-mediated currents). This addition slightly depolarized the cell, functioning as an average for the expected tonic drive. Real tonic drive has more variability than this average, but since it is a summation of several tonically spiking asynchronous cells, the net result is effectively the same.

Connecting the Network

Simulations run in Butera, et al. (1999, *Populations of Coupled Pacemaker Neurons*) demonstrated that there was no significant difference between simulations run with 50 cell populations and simulations run with 500 cell populations. As a result, populations of 50 cells each were used for the Raphe cells, the

pre-BotC cells, the preMNs, and the MNs.

In order for the raphe cells to provide a realistic drive to other cell populations, they must fire asynchronously. The level of artificial stimulation to the raphe cells was varied slightly to accomplish this. After distributing this parameter, the average voltage of the raphe cells demonstrated that asynchronous activity had been achieved:

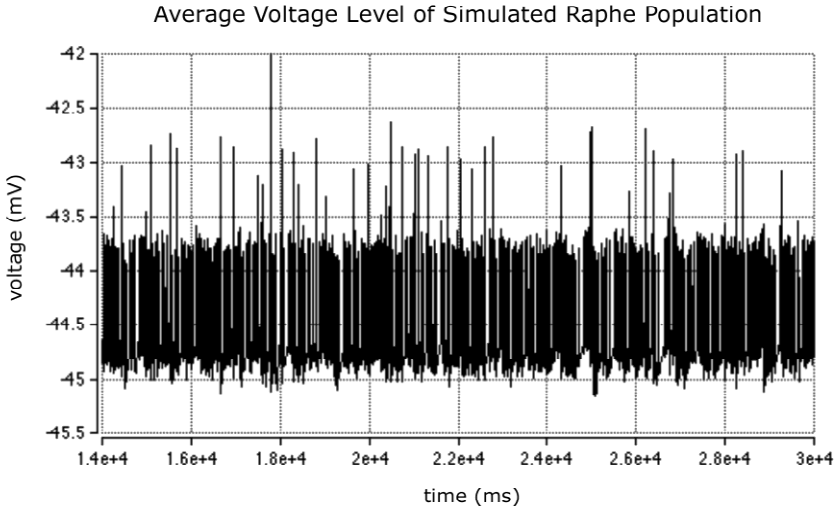

After creating all of the necessary neurons, the connections formed between different neurons must take into account synaptic behavior. The synaptic model used to connect the main three neuronal populations is presented in Butera, et al. (1999, *Populations of Coupled Pacemaker Neurons*). This fast-acting glutamatergic model introduces a current term in the postsynaptic cell defined by:

$$I_{syn}=g_{syn}s(V_{presyn}-E_{junction})$$

where g_{syn} is normally distributed around a particular mean for each population and s describes a gating variable that is driven by presynaptic depolarization. $E_{junction}$ was set at 0 mV, as is expected for EAA-mediated synaptic currents. The synaptic conductance coefficient for pre-BotC cells was randomly chosen, and based off of estimates used in Butera, et al. (1999). The values for g_{syn} in the preMNs and MNs were estimated based on voltage-clamp I_{syn}/C_m measurements from Koizumi, et al. (2008). By solving $I_{syn}/C_m=g(V-E_{syn})/C_m$, with V equal to -65 mV (voltage level during experiment) and E_{syn} equal to 0 mV, the resulting conductance coefficients for the preMNs and MNs were 1.88 and 3.51 nS.

The serotonergic raphe synapses initiate a G-protein second messenger cascade in the post-synaptic neuron, causing channels to open. Since more specific data is not available, this connection was modeled after the $GABA_B$ receptor put forth in Golomb et al. (1996). The effect of this synapse is to introduce a term of the same form as the glutamatergic synapse above, while also modulating the leak currents of the post-synaptic cell. The ion selective channels that open during signal propogation cause a much higher sodium contribution to leak, driving the overall reversal potential for leak higher (to -30 mV). The values used for the synaptic connections between the raphe neurons and the pre-BotC kernel were based on experimental results. In order to correctly extend the raphe stimulus to the MNs, the conductance coefficient of the synapse was scaled by the capacitance ratio of the MN to the pre-BotC cell.

The final steps in order to complete the network, since the cells and their synaptic connections have been appropriately modeled, are to realistically distribute necessary parameters and to define the synaptic connection probabilities between different cell groups. Some of the relevant parameters for this network were set as follows:

Final Network Parameters*

	Raphe cells	pre-BotC cells	preMNs	MNs
g_{NaP}	1.26	2.15, std 0.43	1.26	2.5
g_{leak}	4.7	-	4.14	9.36
g_{INa}	-	0.4	-	-
g_{IK}	-	2.2, std 0.4	-	-
g_{Na}	561.75	28	561.75	1109.5
g_{K}	1043.25	11.2	1043.25	2060.5
g_{A}	833	-	802.5	1585
g_{H}	4.0125	-	4.0125	7.925
g_{P}	1000	-	40.125	79.25
g_{N}	40.125	-	40.125	79.25
g_{T}	16.05	-	16.05	31.7
g_{SK}	200	-	240.75	475.5
g_{tonic}	6.93	0.13	6	15
g_{syn}		0.1, std 0.02	1.88, std 0.4	3.51, std 0.8
$g_{syn, raphe}$	-	25.64	-	77.41

*all values in nS

The matrix used to indicate cell connectivity were generated in Microsoft Excel and copied into the model to avoid variability between trials. Because the actual connectivity among and between groups is unknown, this matrix was varied throughout the process in order to achieve robust signal transfer. In the most complete version of the model, the raphe and pre-BotC cells were connected to each other in an all-to-all configuration, while the preMNs and MNs had a 20% probability of forming synaptic connections within their groups. The probability of pre-BotC neurons forming connections with preMNs, or preMNs connecting to MNs, was set at 50%. The pre-BotC was connected to the MNs with a probability of 10%, because through-connections of this type have been observed. The raphe cells were set to an all-to-all configuration with the two groups they stimulated: the pre-BotC neurons and the MNs. Though it hasn't been verified, it is probable that the raphe input also extends to the preMNs. In this model, though, this connection probability, along with all other connections that haven't been mentioned, was set to 0%.

Results and Discussion

To verify that the model was correct, both individual cell properties and network properties were tested. Comparison between real and simulated action potential waveforms in the raphe reveal that the general shape was preserved, though more tuning is required to capture the subtleties of the wave (see figure below).

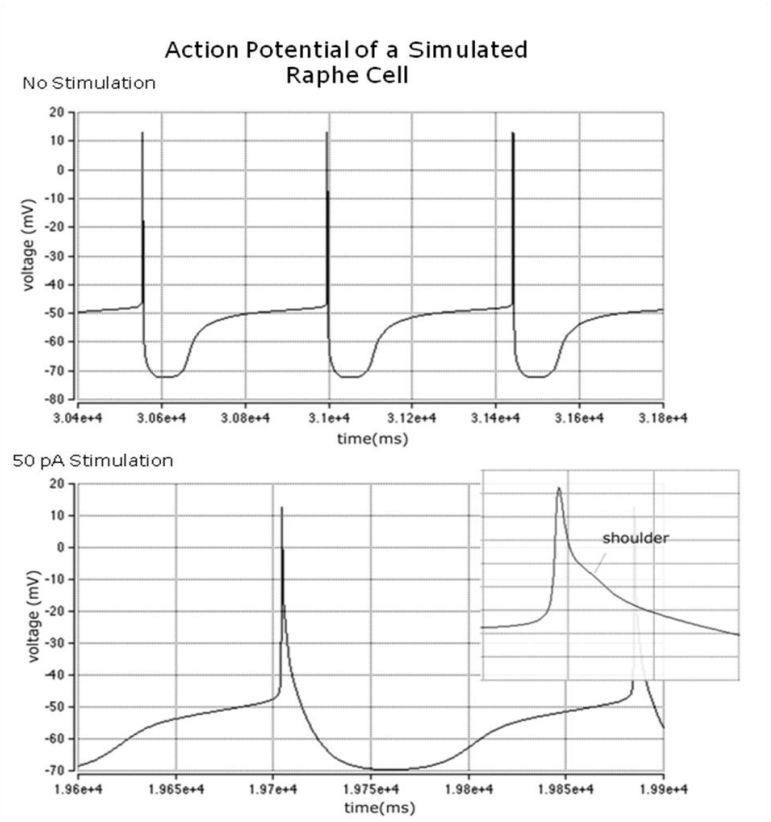

A similar comparison of the our preMN and MN waveforms to the original model waveform demonstrate that these cells still capture the essential features of the action potential (see figure below).

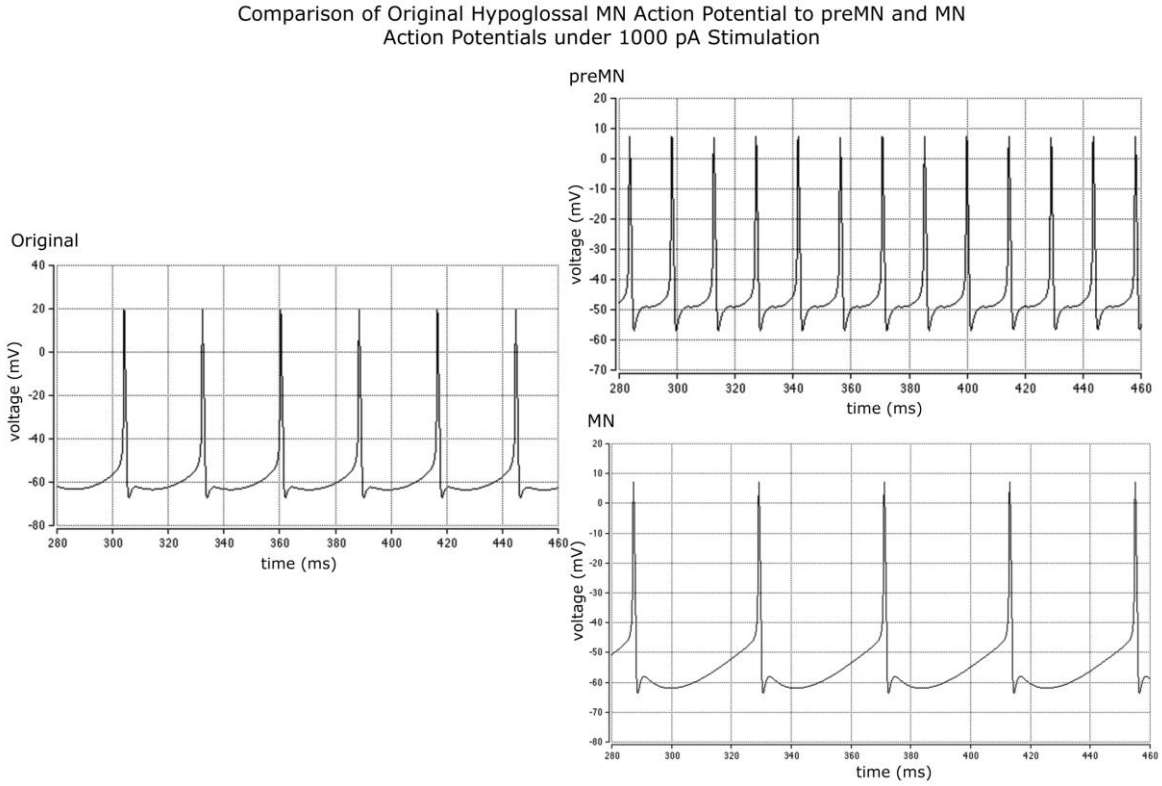

Another feature that is used to verify that cell models are working correctly is the F-I curve, created by artificially stimulating the cell and graphing the resulting spike frequency against the applied stimulation. Experimental raphe data showed a slow adaptive behavior when the stimulation level was changed— in this analysis, however, adaptation was not considered. The steady-state F-I curves of experimental raphe cells and the F-I curve of the simulation are very similar, both monotonically increasing from around two to five hertz as a result of 10-50 pA stimulation (see figure below).

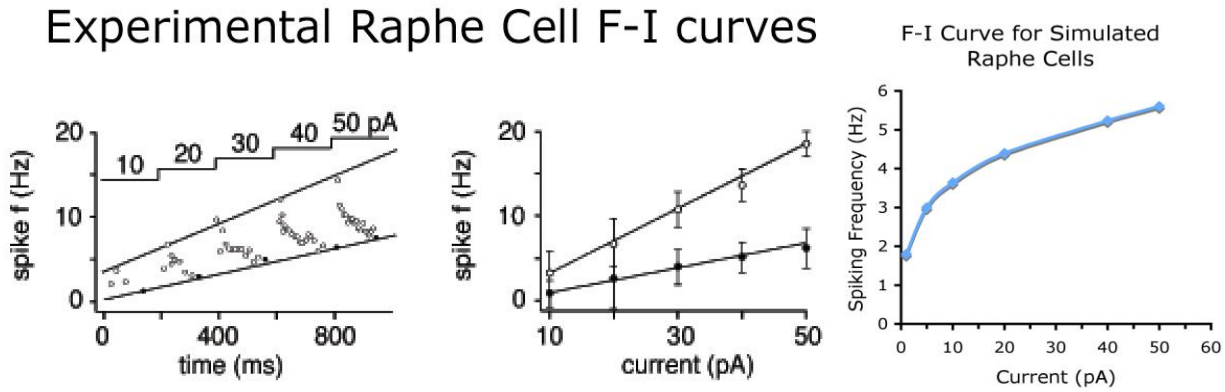

Comparison of the F-I curves of the preMNs and MNs revealed a less similar relationship. Spiking frequency varied widely between experimental and simulated neurons, suggesting more experimental data is necessary to better model these cells. Even so, the linear F-I relationship is preserved in our simulation, and these two figures have similar slopes (see figure below).

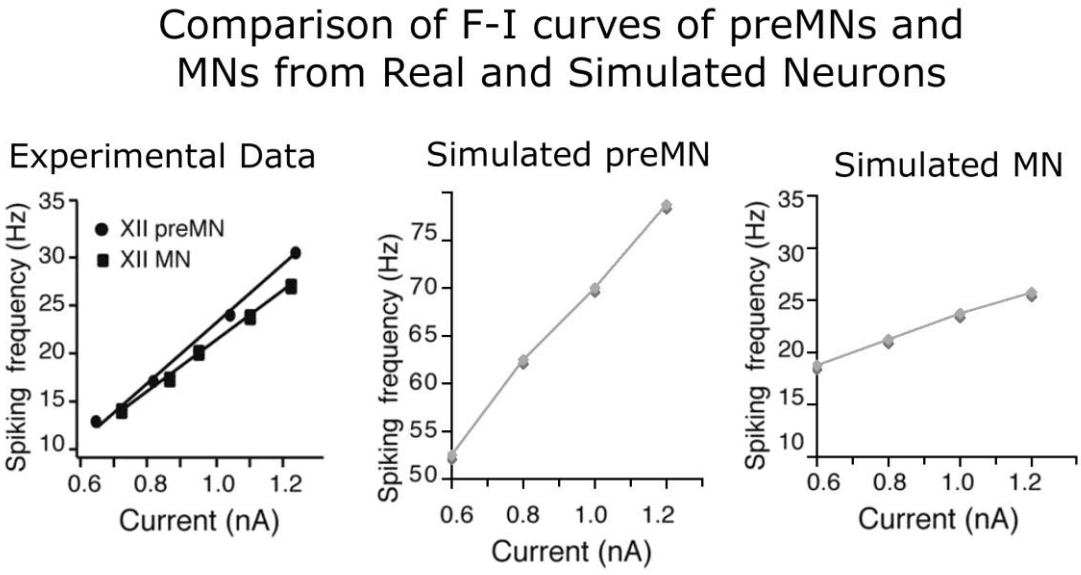

Average population voltage and property interdependence were used to verify that the populations were interacting properly. The raphe cells were shown to fire asynchronously by considering the average voltage of the population (see *Methods and Materials* section). Once this was verified, the raphe neurons were connected to preBot-C cells, and this relationship was tested. As expected, changes in the raphe single cell firing frequency resulted in a similar change in the bursting frequency of the pre-BotC (see figure below).

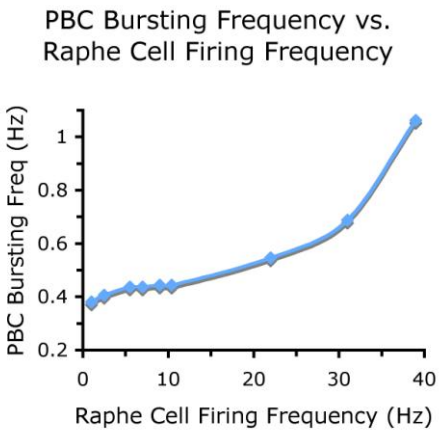

Finally, network transmission of the bursting pre-BotC population was checked. Raster plots were calculated, which represent bursting behavior with a red mark for each individual cell, along with the corresponding histogram, revealing successful transmission to the MNs. By monitoring the average voltage level of each population during a simulation, this transmission of the original signal was corroborated (see figures below).

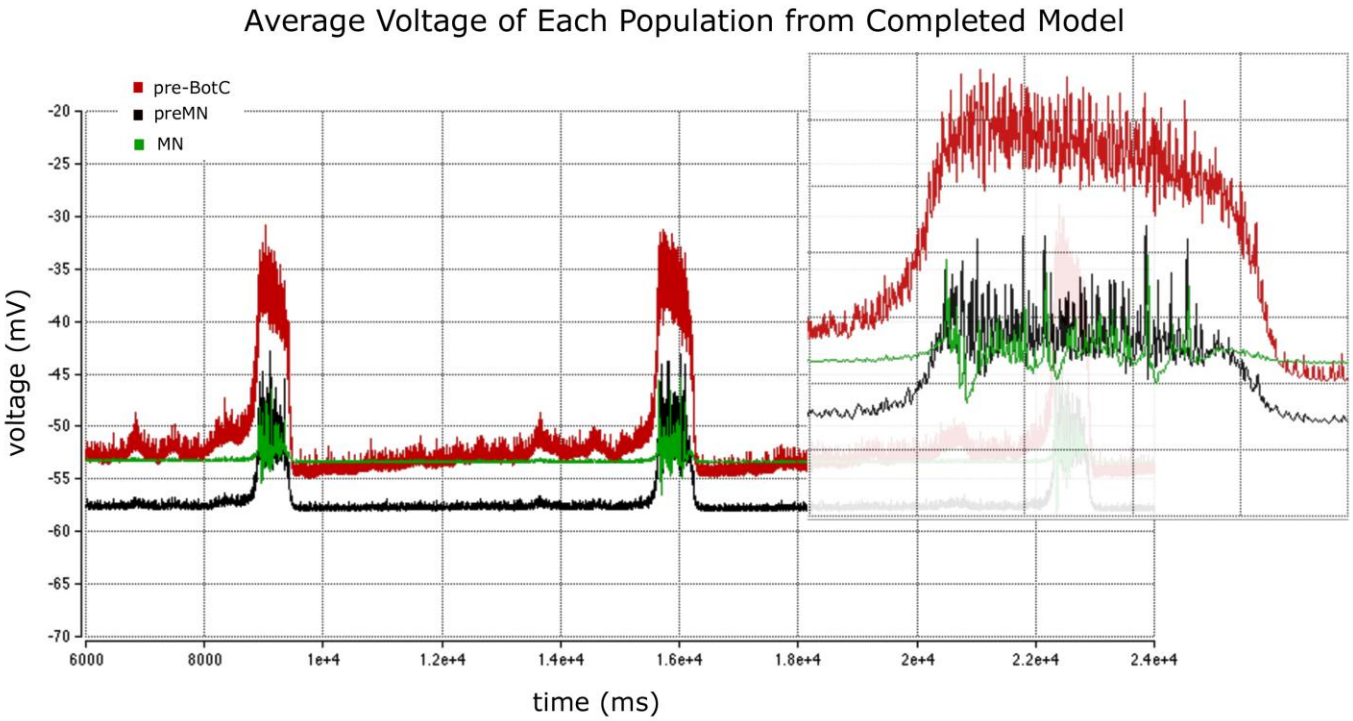

Raster Plots and Spike Frequency Histograms of the Completed Network

pre-BotC

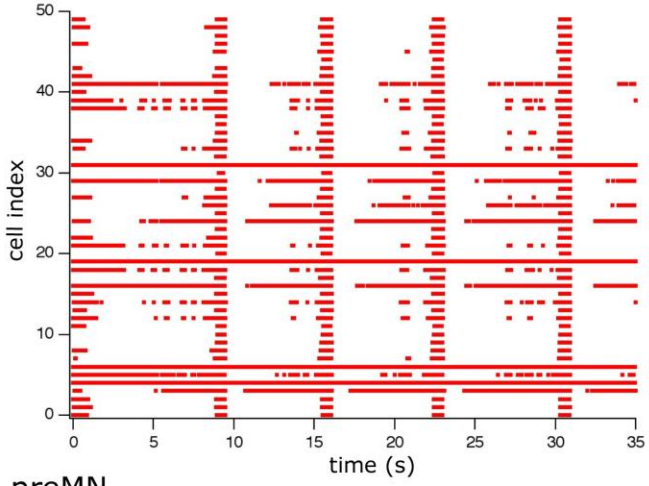

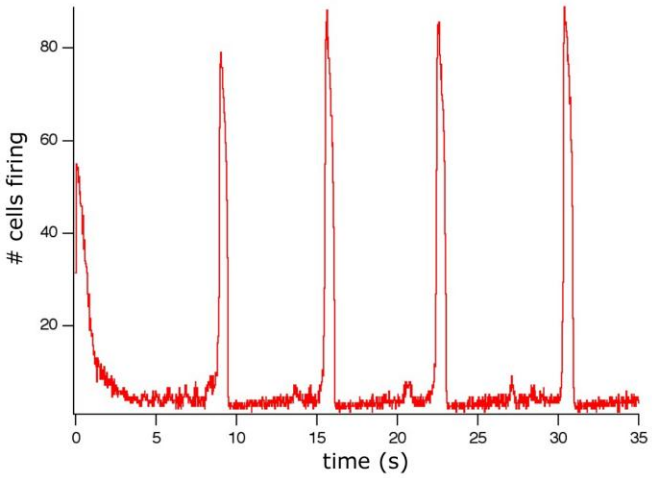

preMN

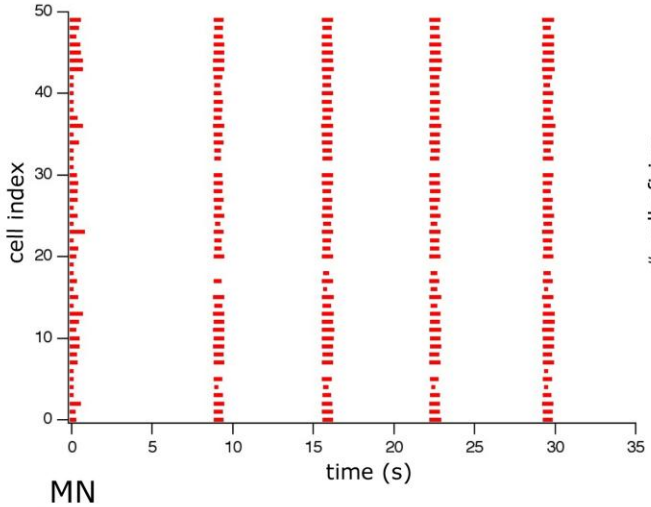

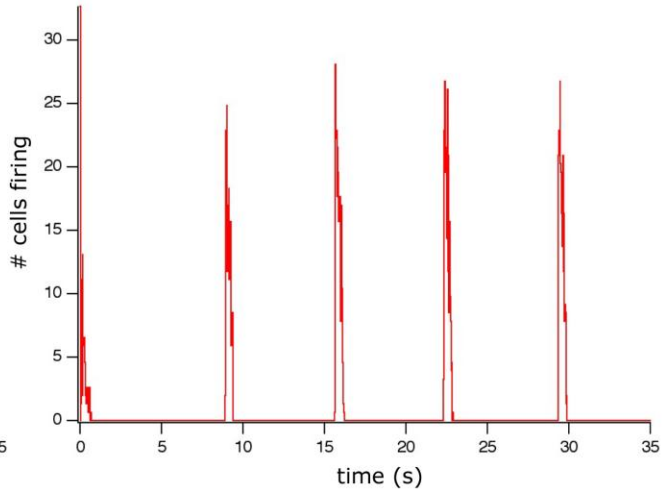

MN

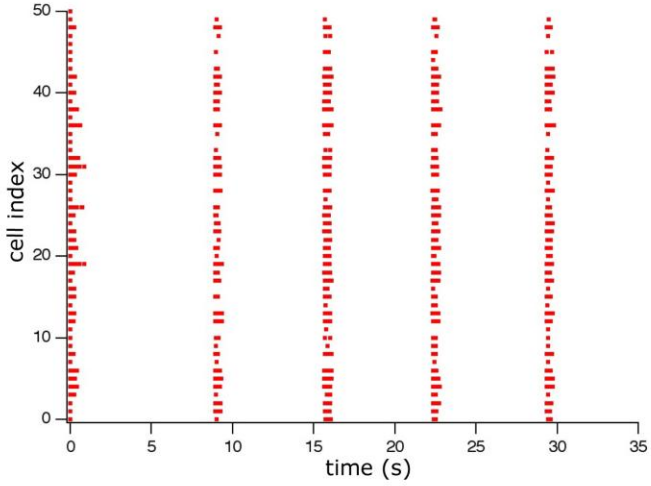

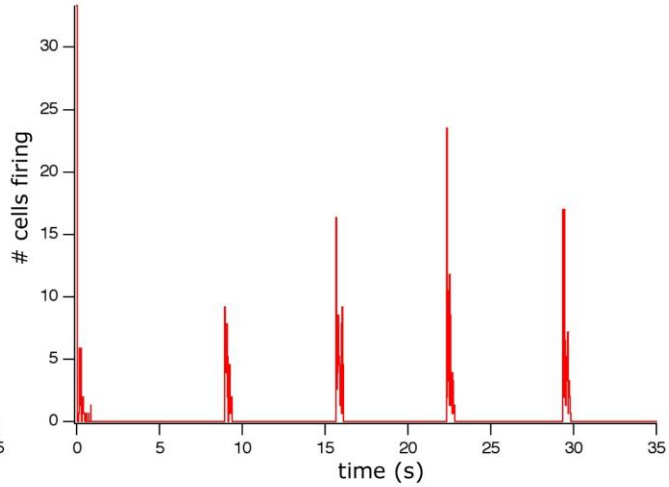

These results indicate that simulated cells retained most of their defining characteristics, though the cell models could be further refined. Dynamic network interaction was successfully recreated, and insight into this complex system is possible. Further refinement of the model and more experimental data can be incorporated in order to further our understanding of neuron interaction.

Conclusion

This computational model represents a large-scale network of the respiratory system in the mammalian brain. Though it is in need of improvement and further development, the basic framework is functioning and capable of realistically replicating certain features of the system as observed experimentally. As more data becomes available and aspects of this model are refined to better approximate the complex interactions of this system, new insight into network dynamics and neuronal interdependence will be gained. In addition, it will be possible to study and model the large-scale effects of pharmacological changes in great detail. While the modeled components represent a very specific system, the principles of network interaction apply to all populations of neurons, and the underlying structure presented here could easily be altered to reflect other specialized systems. This prototype, though still in need of revision, represents the first step toward a fully functional model of a complete neuronal network.

References

BUTERA, R. J., RINZEL, J., AND SMITH, J. C. Models of respiratory rhythm generation in the pre-Botzinger complex. I. Bursting Pacemaker Neurons. J. Neurophysiol. 82: 382–397, 1999.

BUTERA, R. J., RINZEL, J., AND SMITH, J. C. Models of respiratory rhythm generation in the pre-Botzinger complex. II. Populations of coupled pacemaker neurons. J. Neurophysiol. 80: 398–415, 1999.

GOLOMB, D., WANG, X-J., AND RINZEL, J. Propgation of spindle waves in a thalamic slice model. J. Neurophysiol. 75: 750–769, 1996.

KOIZUMI, H., WILSON, C. G., WONG, S., YAMANISHI, T., KOSHIYA, N., AND SMITH, J. C. Functional Imaging, Spatial Reconstruction, and Biophysical Analysis of a Respiratory Motor Circuit Isolated *In Vitro*. J. Neurosci. 28(10): 2353–2365, 2008.

PURVIS, L. K., AND BUTERA, R. J. Ionic Current Model of a Hypoglossal Motoneuron. J. Neurophysiol. 93: 723–733, 2005.